Astron. Astrophys. 188, 145–154 (1987)

ASTRONOMY
AND
ASTROPHYSICS

Observation of cosmic ray positrons in the region from 5 to 50 GeV

R.L. Golden[1], S.A. Stephens[2], B.G. Mauger[1], G.D. Badhwar[3], R.R. Daniel[2], S. Horan[1], J.L. Lacy[3], and J.E. Zipse[3]

[1] Particle Astrophysics Laboratory, P.O. Box 3-PAL, New Mexico State University, Las Cruces, NM 88003, USA
[2] Tata Institute for Fundamental Research, Homi Bhabba Road, Bombay 400005, India
[3] National Aeronautics and Space Administration, Johnson Space Center, Houston, TX 77053, USA

Received March 9, accepted May 25, 1987

Summary. The absolute flux of cosmic ray positrons has been measured using a balloon-borne magnet-spectrometer. Based on 193 positrons observed from 3.57 GV/c to 50 GV/c rigidity at the payload, the integral flux about 5 GeV kinetic energy at the top of the atmosphere is found to be $(0.33 \pm .07) e^+/m^2$-str-s. At the top of the atmosphere the effective energy interval for the observation is 4.5 to 64 GeV. In this interval the best-fit differential flux is $16E^{-(3.0\pm0.3)} e^+/(m^2$-str-sec-GeV). The quoted errors do not include a possible 10% systematic uncertainty in the exposure factor. The ratio $e^+/(e^+ + e^-)$ was found to be 0.069 ± 0.014 above 5 GeV. We compare these results with other observations and theoretical predictions.

Key words: Cosmic rays – general – positrons, electrons.

1. Introduction

Positrons (e^+) with energies above a few hundred MeV are expected in the cosmic rays due to decay of mesons produced by collisions of cosmic rays with the interstellar medium. Particles resulting from such collisions are generally referred to as secondaries. The parents of secondary positrons of energy E are principally protons with an energy of about $10E$. Once produced, the e^+ undergo radiative energy losses as they propagate through the electromagnetic fields of the interstellar medium. Secondary nuclei such as Li, Be and B are produced at the same energy/nucleon as their parents and do not undergo significant radiative energy losses. Consequently, positron observations are capable of giving new insights about cosmic ray phenomena. It should be noted that antiprotons ($\bar{p}$) are also expected to be produced as secondaries of protons of $\approx 10x$ higher energies but are not subject to radiative energy losses. Thus comparison of e^+ and $\bar{p}$ fluxes should yield interesting constraints for the various models of cosmic ray production and propagation (e.g. Badhwar and Golden, 1974).

The data presented here were gathered during a balloon flight from Palestine, Texas on May 20, 1976. The apparatus floated beneath an average of 5.8 g cm^{-2} of atmosphere for a period of $6.4\,10^4$ s. There was a total of 0.16 radiation lengths of material in the atmosphere above the payload and 0.08 radiation lengths of material above the spectrometer in the payload. Electrons (e^-) gathered during the same flight have been reported in Golden et al. (1984a), hereafter referred to as "the e^- paper." The e^- paper contains extensive details on the calibration of the instrument, detection efficiencies, and validation of absolute fluxes measured with the instrument.

This same instrument was used in a later flight to measure the $\bar{p}/p$ ratio (Golden et al., 1979). It is the opinion of the investigators that the e^+ observation is a substantially more difficult task than the $\bar{p}$ observation. The most powerful asset of a magnet-spectrometer is its ability to directly distinguish charge. For negatively charged particles, one has to distinguish $\bar{p}$ from a 20 times higher flux of e^- and from atmospheric mesons. In the case of e^+, however, one must separate the desired particles from protons, which have the same charge and a flux nearly 1000 times as great. The approach taken here was to first apply the selection criteria of the e^- paper to the positively charged events. This yielded a sample which was roughly 25% positrons and 75% protons. Additional criteria were then applied to the Cherenkov-detector and shower-counter responses to further reduce the proton content. The efficiency of these selection criteria was measured by their effect on the e^- events. The remaining proton background was determined by further shower-counter analysis. The net result, presented here, is an observation of e^+ with well known background content and well known selection efficiencies. The $e^+/(e^+ + e^-)$ ratio has also been determined but the emphasis in the analysis was to determine the absolute e^+ flux.

In this paper the units of magnetic rigidity (momentum/charge) or its inverse (called magnetic deflection) are used when referring to particles at the payload, and units of energy are used when referring to particles at the top of the atmosphere. Energies and fluxes are corrected to the top of the atmosphere, taking bremsstrahlung energy losses into account.

2. The apparatus

The magnet spectrometer has been described previously (Golden et al., 1978). The detector elements were: (1) a gas Cherenkov detector (called G) with a threshold Lorentz factor of 40, (2) scintillators S1 and S2 for charge measurement; (3) eight multiwire proportional counters (MWPC); and (4) a shower counter comprised of seven scintillators (P1–P7), each separated by 1.2 radiation lengths of lead. Signals from all scintillators and G were pulsed-height analyzed. The MWPC utilized the distributed delay-line technique described in Lacy and Lindsey (1974). Each

Send offprint requests to: R.L. Golden

MWPC readout consists of two time values, one from each end of the line. The difference of the values gives the position of a particle, and the sum should be equal to the total delay in the delay line. The time-sum acts as a reliable check on data validity. In this paper, a "good" MWPC measurement is defined as one which has an acceptable time-sum.

The magnet was operated at a current of 120 amps, producing a magnetic field of 10–40 KG-in the MWPC region. The instrument had a maximum detectable rigidity of 80 GV/c. All events satisfying the trigger criteria S1 · P1 · P7 were accepted for transmission to the ground where they were recorded. The geometry factor of the instrument was $324 \pm 5\,\mathrm{cm}^2$-str, and the life time fraction was 0.80.

3. Data analysis

The initial data selection criteria are almost identical to that used in the e^- experiment. The reader is referred to the e^- paper for a detailed discussion. The criteria were:

a. At least 5 x-axis (axis of curvature) and 3 y-axis MWPC readouts have good time-sums. In addition, at least one MWPC in each of the top, middle, and bottom MWPC pairs have good time-sums. And, the MWPC data must fit to a valid trajectory with $\chi_x^2 < 50$ and $\chi_y^2 < 30$.

b. The pulse heights in S1 and S2 must correspond to a charge of $Z < 1.8I_0$, where I_0 is the pulse height of a singly charged relativistic particle.

c. The sum of the pulse heights in P1–P7 must correspond to at least $50I_0$. This criterion corresponds to one fourth the shower size typically associated with a 5 GeV electron.

d. The G counter must be triggered (the minimum signal amplitude correspond to 0.25 photoelectrons).

The first criterion differs slightly from the criterion used in the e^- paper. The e^- criterion required that both bottom MWPC have good time sums, rather than having one good MWPC from each of the three pairs. The revised criterion was developed during the analysis of the $\bar{p}$ flight. It gives a 13% higher MWPC selection efficiency and an improved discrimination against spurious events.

For an ideal experiment, positive curvature events passing criteria (a)–(d) would all be positrons. Protons would all be rejected by criterion (d). Unfortunately the G counter had a very high noise rate. In addition, Cherenkov light generated in the lucite mirror backing could sometimes leak through the mirror coating. The net result was that ~0.5% of protons below the Cherenkov threshold were accompanied by a G pulse. Such protons are referred to as having an accidental G-pulse.

Figure 1a shows the deflection distribution with the above criteria. The peak near zero-deflection is due to protons above the Cherenkov threshold. The gradual rise with increasing positive deflection is due to the combination of protons below Cherenkov threshold (accompanied by an accidental G-pulse) and positrons. The decline above 0.2 GV/c is due to the geomagnetic cutoff. The events to the left of zero deflection are the e^-. They also show the geomagnetic cutoff (at around −0.24 GV/c). Because of criterion (c), the protons in this sample must have undergone at least a small interaction in the shower counter. The data at this point have been selected with the same exposure factors as in the e^- paper except for a factor 1.13 due to the change in criterion (a).

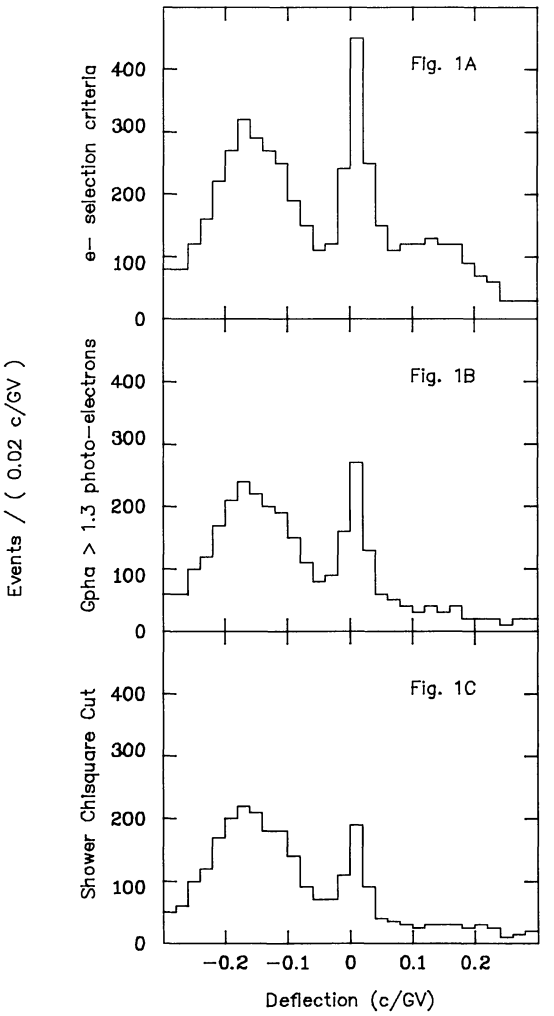

Fig. 1. Effects of selection criteria. Figure 1A shows the deflection spectra of events selected by applying the criteria basically used for recognizing e^-. The criteria included tests for quality of the trajectory information, a charge of 1, at least a small cascade in the shower counter, and at least a small signal from the Cherenkov detector. Figure 1B shows the effect of raising the minimum Cherenkov pulse-height requirement to the equivalent of 1.3 photoelectrons. Figure 1C shows the effect of further requiring that the cascade fit the form of an electromagnetic cascade with a χ^2 of less than 10.0

In order to further reduce the proton background, additional criteria have been imposed. Separate samples of protons and electrons can be derived from the data to develop new criteria and evaluate their efficiencies. For example, selection efficiencies for positrons can often be measured using the e^- sample selected with criteria (a)–(d). Similarly, one can obtain a sample of protons by imposing only criteria (a)–(c), and using positive curvature events (such a sample will contain more than 99.7% protons). Electrons (e^-) and protons were selected using these techniques and were then used to evaluate additional G-counter selection criteria.

G-counter accidental pulses are usually due to single photoelectrons. Furthermore, the noise pulses are emitted from the photocathode at random times relative to the event trigger. Thus the below-threshold protons should be greatly suppressed by

requiring a larger G pulse height. An appropriate pulse height test was devised by comparing the G pulse-height distribution of protons below Cherenkov threshold with the pulse-height distribution for the e^-. The G pulse-height selection criterion was chosen to be:

e. The G pulse-height must correspond to at least 1.3 photoelectrons.

Studies of the appropriate proton and electron distributions show that this criterion removed about 70% of the proton background. The criterion rejected about 21% of the e^- sample and can be assumed to reject the same fraction of e^+. Figure 1b shows the deflection distribution of events passing criteria (a)–(e). One can notice a sharp decrease of the proton peak in the positron deflection region, with a less noticeable change in the corresponding e^- distribution.

The shower counter data must be examined to further discriminate between protons and e^+. Once again, a valuable aid is to study protons and e^- gathered from the flight. At rigidities below 40 GV/c, a sample of protons for use in shower counter studies can be obtained by selecting positive particles that satisfy criteria (a)–(c) and have G off. The expected e^+ shower responses can be obtained from a sample of electrons gathered by using events with negative curvature satisfying criteria (a)–(e). The P1–P7 pulse heights from both the proton sample and the e^- sample were fitted to the hypothesis that the shower was an electromagnetic cascade. The starting point and total energy of the cascade were free parameters in the fit. These two parameters plus the χ^2 for the shower fit constitute the remaining information to be used in distinguishing the positrons from the protons.

One would expect that the proton shower fits would have a higher average χ^2 than the electron fits. This indeed was observed to be the case. Criterion (f) was chosen to be:

f. The shower profile of an e^+ candidate must fit with a χ^2 of less than 10.0.

This criterion rejected about 80% of the remaining protons and about 5% of the electrons. Figure 1c shows the deflection distribution of events passing criteria (a)–(f). It can be seen that there is a considerable reduction of the protons in the selected sample.

A total of 409 events with positive charge and rigidities less than 50 GV/c passed the selection criteria. These events are called e^+ candidates. As in past presentations of this data, we investigated the amount of proton background remaining in the e^+ candidates by examining the distribution of cascade starting points in the shower counter, and by analyzing the total shower amplitude. The next section describes the determination of the proton background in the e^+ candidates by analyzing the starting-point distributions.

3.1. Starting point method

In order to get an idea of the starting point distribution expected for e^+, one can examine the starting point distribution of e^-. The e^- starting-point distributions are energy independent. Figure 2 shows the e^- starting point distribution for e^- that pass criteria (a)–(f). Proton starting point distributions are slightly energy dependent. Figure 2 contains a typical proton starting-point distribution for comparison. The e^- distribution is roughly Gaussian with a width of about 1 radiation length (i.e. $1X_0$) and a peak at $+1X_0$. The $+1X_0$ offset is an artifact of the shower fitting program. Starting points greater than $+1X_0$ correspond

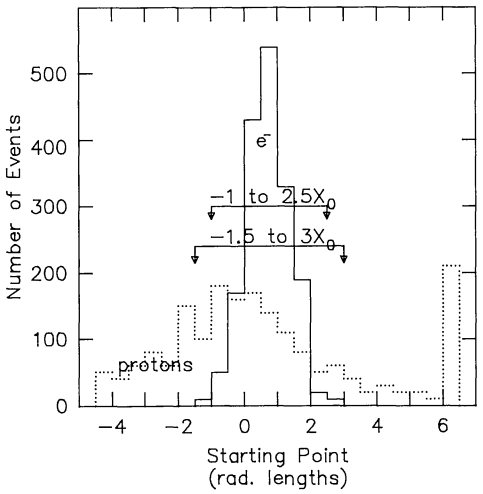

Fig. 2. Starting-point distributions for e^- and protons. Each cascade is fitted to the form of an electromagnetic cascade. Energy and starting point are used as free variables in the fit. This figure shows the starting-point distributions for e^- and protons. Note that the proton starting-point distribution is considerably broader than that observed for e^-. The peak at the right side of the proton distribution is due to the fact that often the only way to fit a proton cascade as an electromagnetic cascade is to assume that the measurements are actually the tail of an electromagnetic cascade occurring well above the shower counter. The fitting program tried only starting points between -7 and $+6X_0$

to showers initiating above the shower counter, and those between $+1X_0$ and $-7X_0$ start within the shower counter. It can be noticed that there are no e^- events beyond the interval $-1.5X_0$ to $3X_0$, and only 0.5% of the events fall outside the interval $-1.0X_0$ to $2.5X_0$.

The proton distribution is clearly broader than the e^- distribution. The broad peak in the proton distribution is due to a bias introduced by the requirement for a minimum shower size. The peak at $+6X_0$ is because the shower fitting program tries to fit proton interactions in the top layer as the tail end of a shower occurring well above the shower counter. The $+6X_0$ point is the most positive point analyzed by the fitting program. We exploit the general differences in proton and electron starting-point distributions to determine the amount of remaining proton contamination in the positron sample.

Figure 3 shows the starting-point distribution for protons and e^+ candidates at two different rigidity intervals. It can also be noticed that the number of e^+ candidates which fall outside the region between $-1.5X_0$ and $3.0X_0$ is smaller for the low-rigidity interval (5.0–6.25 GV/c) than for the high-rigidity interval (6.25–12.5 GV/c) indicating the presence of more protons in the high-rigidity sample. The events which are outside the interval $-1.5X_0$ to $3.0X_0$ were used to determine the proton background in the e^+ sample by calculating a multiplying factor M = (total protons)/(protons outside the starting point limits). The total background in the e^+ sample was estimated as the number of early and late showers multiplied by M. Table 1 shows the determination of M for a number of rigidity intervals.

In order to evaluate the effects of the background subtraction, one can examine the starting-point distribution of the e^+ events after the background subtraction. Figure 4 shows data for the same rigidity intervals as Fig. 3. The solid histograms in Fig. 4 are for e^- events and the dashed histogram is for e^+.

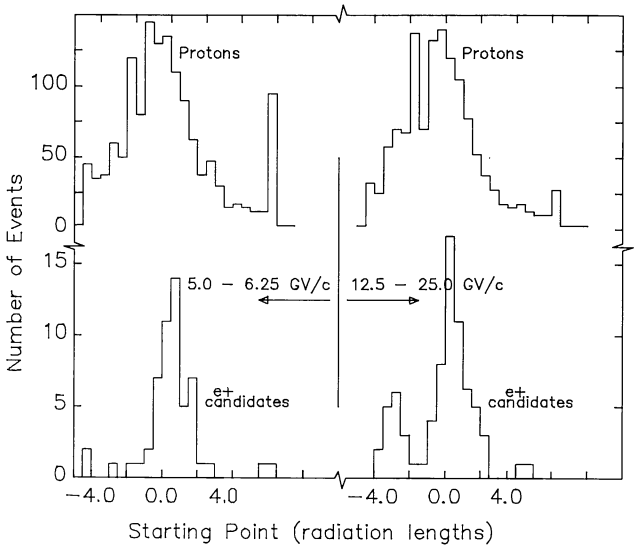

Fig. 3. Starting-point distributions of e^+ candidates. Starting-point distributions for the e^+ candidates and protons are shown for two rigidity intervals. In the low-rigidity interval the starting-point distribution of the e^+ candidates appears to be dominated by a narrow peak near zero radiation lengths typical of electrons (see Fig. 2). The high-rigidity interval clearly has a significant proton-like component

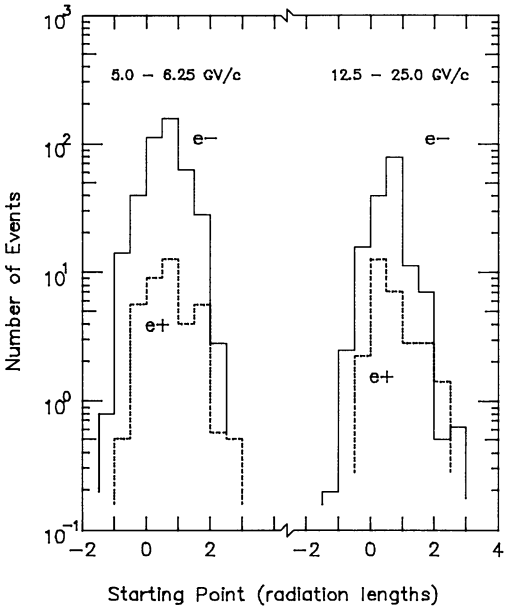

Fig. 4. Starting-point distributions for e^+ and e^- after background subtraction. The e^+ and e^- distributions are very much alike. Note that neither distribution has counts beyond the interval $+3X_0$ and $-2X_0$

Notice the similarity of the e^- and e^+ histograms, which gives the confidence that the remaining sample is really positrons. In the past analyses of this data (Golden et al., 1985), we did not examine the starting-point distribution after background subtraction. Such an examination would have revealed that our past use of a very wide range of starting points (-2.5 to $+3.5X_0$) was leading to over-subtraction of the background which was manifested by large regions of negative count-rate in the equivalent of Fig. 4. The choice of large starting-point interval for separating protons from positrons was made simply to assure that no positrons were lost. Figure 2 shows that the starting-point interval used in the earlier analyses was unnecessarily large.

Table 1. Computation of the background multiplier M

This table illustrates the determination of the background multiplier for the assumption that events with starting points outside the interval $-1.5X_0$ to $3.0X_0$ are all protons. If N_{ptot} is the total number of proton events in a particular rigidity interval, and N_{pout} is the number of these events which are outside the above mentioned starting point interval, then the background multiplier is $M = N_{ptot}/N_{pout}$. Computation of the uncertainty in M must incorporate the fact that N_{ptot} abd N_{pout} are not statistically independent. The error in M is given by $\Delta M = [M(M-1)/N_{out}]^{1/2}$.

Rigidity	N_{ptot}	N_{pout}	M
3.57–4.17	138	52	2.65 ± 0.29
4.17–5.00	535	209	2.56 ± 0.14
5.00–6.25	1393	562	2.48 ± 0.08
6.25–8.33	1775	733	2.42 ± 0.07
8.33–12.50	1636	620	2.64 ± 0.08
12.50–25.00	1252	489	2.56 ± 0.09
25.00–50.00	372	152	2.45 ± 0.15

The use of a large selection interval resulted in small numbers of events outside the criterion in the positron sample. This greatly increased the sensitivity of the results to fluctuations in the proton statistics.

In light of our past errors in selecting the correct range of starting points, it is useful to examine whether the background removal process used here is sensitive to reaonable changes in the choice of starting-point cuts. For this purpose we determined the value of M using proton events outside the interval $-1.0X_0$ to $2.5X_0$. Using the e^- sample, it was found that only 0.5% of the electrons (or positrons) would be lost even with this very narrow cut (Fig. 2). The $-1.0X_0$ to $2.5X_0$ selection criteria gave $191e^+$ after background subtraction while using the $-1.5X_0 + 3.0X_0$ criterion gave $193e^+$. Table 2 gives the details of the $-1.5X_0$ to $3.0X_0$ starting point analyses. Table 3 contains the results of both analyses. The consistency of the two analyses demonstrates that the results are not sensitive to the selection criteria. Note that Table 2 indicates that for the three highest rigidity intervals, the majority of the observed events are proton background.

The next section describes an alternative approach to background subtraction based on the size of the cascade in the shower counter.

3.2. Shower sum method

Alternative approaches to subtracting the background could be based on using the total shower amplitude. One such approach was used by Golden et al., 1984a, who used the sum of the shower counter pulse-heights which they called PSUM. We have performed a similar analysis to that of Golden et al. but found that it resulted in erroneous results when applied to the e^+ candidates. In this section we present this analysis together with a revised analysis which is consistent with the shower starting-point method. The approach used in Golden et al. (1984a), was based

Table 2. Computation of e^+ counts

This table contains the details of the subtraction of the proton background from the e^+ candidate sample using the starting point method described in the text. The number of e^+ candidates in a particular rigidity interval is $N_{e^+\,\mathrm{cand}}$. Events with shower starting points outside the interval -1.5 and $+3.0X_0$ are regarded as being proton events. These events are shown in the column labled N_{out}. To correct for background inside the interval -1.5 to $+3.0X_0$, N_{out} is multiplied by a background multiplier, M determined in Table 1. The computed number of e^+ after proton background subtraction is $N_{e^+} = N_{e^+\,\mathrm{cand}} - MN_{\mathrm{out}}$. The error in N_{e^+} is given by

$$\Delta N_{e^+} = [N_{e^+\,\mathrm{cand}} - N_{\mathrm{out}} + (1-M)^2 N_{\mathrm{out}} + N_{\mathrm{out}}^2 \Delta M^2]^{1/2}$$

Rigidity (GV/c) ρ	Number e^+ candidates $N_{e+\mathrm{cand}}$	Number e^+ outside N_{out}	Background multiplier M	Number e^+ Remaining N_{e^+}
3.57–4.17	28	1	2.65 ± 0.29	25.4 ± 5.5
4.17–5.00	54	3	2.56 ± 0.14	46.3 ± 7.6
5.00–6.25	55	6	2.48 ± 0.08	40.1 ± 7.9
6.25–8.33	60	8	2.42 ± 0.07	40.6 ± 8.3
8.33–12.50	51	14	2.64 ± 0.08	14.0 ± 8.7
12.50–25.00	74	19	2.56 ± 0.09	25.4 ± 10.2
25.00–50.00	87	36	2.45 ± 0.15	−1.2 ± 12.5

on the fact that proton initiated showers have a substantially smaller PSUM than electron initiated showers at the same rigidity. Examination of proton and e^- events reveals that proton initiated showers usually have a PSUM of less than $100I_0$ (I_0 is the pulse-height corresponding to 1 minimum ionizing particle in one layer) for rigidities less than 6.25 GV/c and PSUM less than $150I_0$ for rigidities between 6.25 and 50 GV/c. In contrast, e^- events are always above these PSUM limits. Using these PSUM limits we performed a background subtraction in a manner similar to that used in the starting-point method. Events in the e^+ candidate sample that have PSUM below the limit are regarded as proton events. The background in the e^+ sample was then determined as the number of events below the PSUM limit multiplied by a factor N, where N is the ratio of total protons to protons below the PSUM limit for the corresponding proton sample. Figure 5 shows the PSUM distribution of proton events and e^+ candidates for two rigidity intervals. The e^+ PSUM distribution for the low rigidity sample shows a peak at low PSUM indicating the presence of protons and shows a peak at high PSUM values indicating the presence of e^+. At high rigidities, the PSUM distributions of protons and e^+ are less distinct but the e^+ distribution still shows an excess at large PSUM values. We have then evaluated the proton background in the e^+ sample as described in the starting-point method by making use of the events below the PSUM cut and replacing M by N. After performing the background subtraction, it is useful to compare the resulting e^+ distribution with the corresponding e^- distribution.

Figure 6 shows these distributions for the same rigidity intervals as Fig. 5. It is clear for this figure that in the low rigidity interval the e^- and e^+ distributions are similar. The number of e^+ events (after background subtraction) in this interval is 39.4 ± 7.7 events for the starting-point method and 34.5 ± 6.8 events for the shower-sum method. However, in the higher rigidity interval, one can notice that the PSUM distributions for the

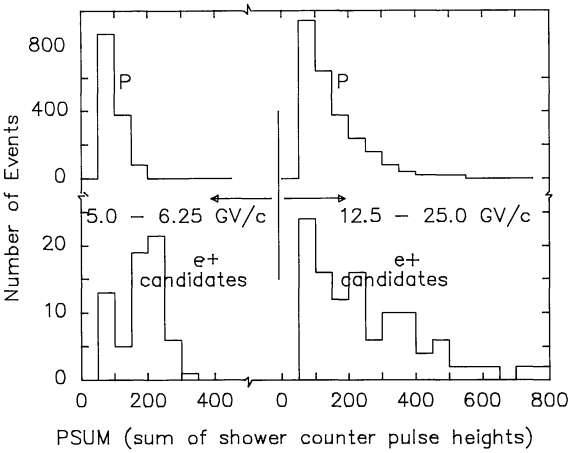

Fig. 5. Shower-sum distributions for e^+ candidates and protons. The low-rigidity samples indicate a substantial difference between the e^+ candidates and the corresponding protons. The e^+ candidates appear dominated by larger amplitude cascades as expected if e^+ are present in the sample. The high-rigidity distributions are very similar though the e^+ candidates have greater proportion of large-amplitude events indicating a presence of e^+. The high-rigidity e^+ sample seems, however, to resemble the corresponding proton sample more closely than at lower rigidities

e^- and e^+ are different, the e^+ distribution having a greater proportion of lower PSUM values. This indicates the presence of protons in the e^+ sample even after background subtraction. In this rigidity interval, the e^+ count is 45.6 ± 7.6 events while the starting-point method gives 28.7 ± 9.6 events. Failure of the background subtraction process could be understood if there were a small correlation between shower-counter pulse-height and G pulse-height. Such a correlation could result from either electrical or physical cross-talk between the detector systems.

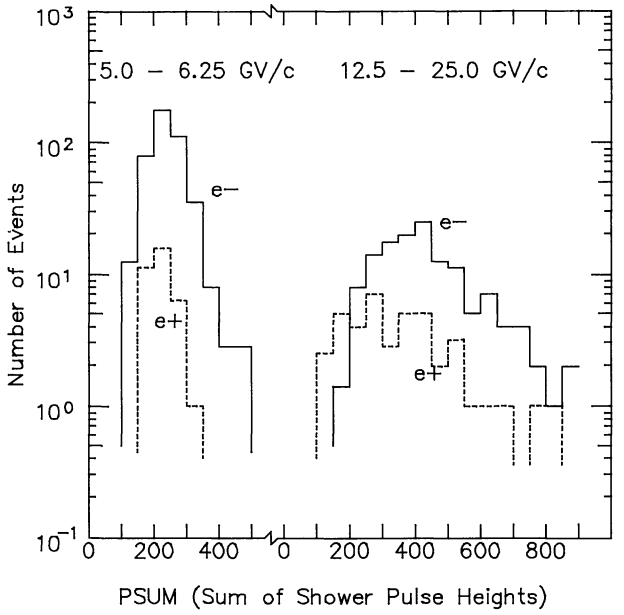

Fig. 6. Shower-sum distributions for e^- and e^+ after background subtraction. The similarity of the low-rigidity e^+ and e^- distributions is indicative that the background subtraction process is reliable. At high rigidities, however, the technique apparently does not work. Note the excess of events with low shower-sum in the e^+ distribution. This indicates the presence of protons even after the background subtraction process has been carried out. Failure of this technique at high rigidities may be due to a small correlation between the shower-sum amplitude and the Cherenkov amplitude causing protons with larger cascades to preferentially be accompanied by a Cherenkov pulse

The effect of the cross-talk would be to allow protons with large showers to meet the minimum G-pulse-height criteria and thus appear in the e^+ candidate sample. Such an effect may not have been apparent in the e^- analysis of Golden et al. (1984a), because the proton background for the e^- experiment is orders of magnitude smaller than for the e^+ experiment.

Another approach to using PSUM information for background subtraction would be to use only showers of large pulse-height and normalize to the e^- distribution. It is apparent from Fig. 6 that beyond the peak in the PSUM distributions the shapes of the e^+ and e^- PSUM distributions are similar. For any particular rigidity interval, we define the most probable value of PSUM for the e^- as P_0. If we ignore the contribution of protons with PSUM $> P_0$, we can estimate the total number of e^+, as the number of e^+ with PSUM $> P_0$ multiplied by a normalizing constant N which is the ratio of the total number of e^- to that with PSUM $> P_0$. This value was found to be in agreement with the number deduced by starting-point method. We used this "large PSUM" correction method for rigidity intervals above 8.33 GV/c where plots of the type used in Fig. 6 revealed evidence of proton contamination after background subtraction. The lower deflection intervals were analyzed using the original PSUM method. The resulting e^+ fluxes are shown as the column labeled "Shower Sum" in Table 3.

It is very encouraging to note from Table 3 that the e^+ fluxes estimated by the two methods give consistent values. Since the starting-point method is more direct and does not incorporate energy dependent criteria, we have chosen it for the final analysis.

Table 3. Results of e^+ background subtractions

This table summarizes the results of the various methods for subtracting the remaining proton background. The column labled "Strt Pt 1" contains the number of e^+ derived using starting point limits of $-1.5X_0$ and $3.0X_0$, see Table 2. The column labled "Strt Pt 2" was derived in the same manner except using starting point limits of $-1.0X_0$ and $2.5X_0$. The column labled "Shower Sum" was derived using the total shower-counter amplitude as described in the text. The number of e^+ in the 25–50 GV/c interval should perhaps have a higher uncertainty than that shown.

Rigidity ρ (GV/c)	Number of e^+		
	Strt Pt 1	Strt Pt 2	Shower sum
3.57–4.17	25.4 ± 5.5	25.8 ± 5.3	22.6 ± 5.9
4.17–5.00	46.3 ± 7.6	47.5 ± 7.4	40.8 ± 8.6
5.00–6.25	40.1 ± 7.9	38.8 ± 7.5	34.5 ± 9.3
6.25–8.33	40.6 ± 8.3	39.3 ± 7.9	40.9 ± 8.7
8.33–12.50	14.5 ± 8.7	14.6 ± 7.6	14.1 ± 11.5
12.50–25.00	25.4 ± 10.2	31.2 ± 9.0	28.2 ± 14.7
25.00–50.00	−1.2 ± 12.5	1.7 ± 10.5	6.2 ± 4.1

The computation of fluxes from the observed counts was done in the same manner as in Golden et al. (1984a) except that the changes in selection criteria were taken into account. The effects of the selection criteria changes were incorporated by reducing the geometry factor in proportion to the number of additional e^- that were lost during the analysis presented here. The errors quoted for the reduced geometrical factor were derived from the square root of number of e^- that were lost in the new selection.

4. Results

As maintained earlier, the e^- paper contains well established e^- absolute fluxes and the related exposure factors (solid angle x exposure time x observation efficiency). The exposure factors for the e^+ observation were obtained by reanalyzing the e^- data using criteria (a)–(f). The ratio of e^- surviving (a)–(f) to the number of e^- reported in the e^- paper gives a correction factor for the exposure factors reported in the e^- paper. Table 4 shows the data from the e^- paper and the e^- data passing criteria (a)–(f). The changes in number of e^- result from a 13% increase in e^- due to the change in criterion 1, 26% decrease due to criteria (e)–(f) and 5% loss due to the background subtraction. On the average the e^+ exposure factors are about 0.8 times the exposure factors of the e^- paper.

The effects of the propagation of e^+ in the atmosphere have been taken into account in order to establish the flux at the top of the atmosphere. First, the expected number of atmospheric secondaries was subtracted using the calculations of Stephens (1981a). Table 5 summarizes the atmospheric background subtraction. Next, the effects of bremsstrahlung in the material above the spectrometer were taken into account. To study the bremsstrahlung losses we assumed a power law spectrum of e^+ at the top of the atmosphere modified by the geomagnetic cutoff. The geomagnetic transmission efficiency was derived from proton and alpha spectra gathered during the same flight. The assumed spectrum was used in a Monte Carlo calculation (Mauger, 1981)

Table 4. Calculation of exposure factors

The exposure factors for the e^+ observation are computed by adjusting the exposure factors reported in the e^- observation (Golden et al., 1984a) in proportion to the number of e^- surviving the e^+ selection criteria. The column labled "e^- 1984" are the number of e^- in Golden et al. (1984a). The column labled "e^- with e^+ cuts" contains the number of e^- surviving the e^+ criteria in this paper. Atmospheric backgrounds were not subtracted from the e^- counts because we wish only to determine the efficiency of the revised selection criteria. The column labled "ϵ" is the resulting efficiency for passing the additional criteria. The columns labled "$A\Omega t$ 1984" and "$A\Omega t$ this work" are the prior and resulting geometry factors. The error in ϵ is $\Delta\epsilon = [e^-_{1984} - e^-_{\text{this work}}]^{1/2}/e^-_{1984}$. The error in $A\Omega t_{\text{this work}}$ is just the propagation of the error in ϵ.

Rigidity ρ (GV/c)	e^- 1984	e^- with e^+ cuts	ϵ	$A\Omega t$ 1984 (m^2-sr-s)	$A\Omega t$ this work (m^2-sr-s)
3.57–4.17	168	148	0.88 ± 0.03	619	545 ± 17
4.17–5.00	323	276	0.85 ± 0.02	619	529 ± 13
5.00–6.25	529	418	0.79 ± 0.02	619	489 ± 12
6.26–8.33	497	372	0.75 ± 0.02	608	455 ± 14
8.33–12.50	401	309	0.77 ± 0.02	597	460 ± 14
12.50–25.00	198	145	0.73 ± 0.04	575	421 ± 21
25.00–50.00	50	17	0.34 ± 0.11	553	188 ± 64

Table 5. Subtraction of atmospheric background

The number of e^+ produced by collisions of cosmic rays in the atmosphere above the payload was calculated using the work of Stephens (1981a). The results of the calculation are shown in the column labled "atmos. bg". The number of e^+ remaining after the background subtraction is given in the far right hand column. The uncetainty in this quantity was determined by combining, in quadrature, the uncertainty in the total observed e^+ and (atmos. bg)$^{1/2}$.

Rigidity ρ (GV/c)	Number of e^+ total	atmos. bg	above bg
3.57–4.17	25.6 ± 5.4	13.4	12.2 ± 6.5
4.17–5.00	44.6 ± 7.6	10.7	33.9 ± 8.3
5.00–6.25	39.4 ± 7.7	8.1	31.3 ± 8.2
6.26–8.33	39.9 ± 7.7	6.8	33.1 ± 8.1
8.33–12.50	14.3 ± 8.1	4.7	9.6 ± 8.4
12.50–25.00	28.7 ± 9.6	3.0	25.7 ± 9.8
25.00–50.00	0.5 ± 11.5	0.4	0.1 ± 11.5

which included energy changes due to the bremsstrahlung process and the effects of the finite resolution of the momentum spectrometer. For each deflection interval at the payload, a corresponding energy interval was computed at the top of the atmosphere by taking into account the average bremsstrahlung energy loss. A propagation efficiency ϵ_p was determined for each interval by computing the ratio of the number of e^+ generated at the top of the atmosphere to the number of e^+ found in the corresponding interval at the payload. The value of ϵ_p was then subjected to a small correction resulting from the effects of e^- propagating in the atmosphere. The correction was computed by simultaneously solving the coupled diffusion equations for propagation of e^+, e^-, and γ-rays in the atmosphere. The e^+ fluxes were then computed as the number of counts above background divided by the exposure factor, ϵ_p, and the width of the energy interval. The results are given in Table 6. Note that the geomagnetic effects are clearly present in the lowest two energy intervals.

The flux values computed in Table 6 can be represented by a power law. The resulting differential energy spectrum for the interval 4.5 to 64 GeV is

$$j_{e^+}(E) = 16E^{-(3.0\pm0.3)} \text{ particles}/(\text{m}^2 \cdot \text{sr} \cdot \text{s}) \quad (1)$$

Equation 1 fits our data with a χ^2 of 4.7 for 7 data points.

Figure 7 shows the differential flux values derived in Table 6 along with results from Buffington et al. (1975) and Faneslow et al. (1964). The curve shown in this figure is the fitted spectrum (Eq. 1). Considering the large errors associated with the other experiments, there appears to be general agreement amongst the observations. One may notice, however, that the results of Buffington et al. are somewhat smaller than ours in the region 5–15 GeV as was noted previously in the e^- paper.

The fraction of positrons $e^+/(e^+ + e^-)$ was estimated for each energy interval by making use of the observed e^- and e^+ using criteria (a)–(f) given in Tables 4 and 5 and correcting for the e^- atmospheric background. Table 7 and Fig. 8 summarize the ratio calculations. The factor φ in Table 7 is the calculated contribution of e^+ from cascading of the e^- in the atmosphere. The calculated $e^+/(e^+ + e^-)$ ratio in the region 5–30 GeV is 0.069 ± 0.014.

The integral flux values above 5 and 10 GeV have been determined to be $(0.33 \pm 0.07)e^+(m^2 \cdot \text{sr} \cdot \text{s})$ and $(0.066 \pm 0.050)e^+/(m^2 \cdot \text{sr} \cdot \text{s})$, respectively. The integral flux above 7 GeV was determined to be $(0.17 \pm 0.05)e^+/(m^2 \cdot \text{sr} \cdot \text{s})$ which can be compared to the value $(0.16 \pm 0.06)e^+/(m^2 \cdot \text{sr} \cdot \text{s})$ reported by Buffington et al. (1975).

It should be pointed out that the spectral index for e^+ is consistent with the value of -3.15 ± 0.2 obtained for e^- in the

Table 6. Flux calculations

This table summarizes the calculations of e^+ fluxes at the top of the atmosphere. The column labled "Number of e^+" is the weighted average of the two starting point analyses in Table 2. The errors are the simple averages of the corresponding errors in Table 2. Computation of the average energy. $\bar{E}$ and the equivalent energy interval ΔE incorporate the average bremsstrahlung energy losses. The propagation efficiency, ϵ_p, incorporates both bremsstrahlung and geomagnetic effects. The computed flux is given by:

$$\frac{\Delta N}{\Delta E} = \frac{N_{e^+}}{A\Omega t * \epsilon_p * \Delta E}$$

where $A\Omega t$ is given by Table 4. The errors in the reported fluxes are derived by least-squares folding of the errors given for each term.

Rigidity ρ (GV/c)	Number e^+	$\bar{E}$ GeV	ΔE GeV	ϵ_p	$\Delta N/\Delta E$ #/(cm^2 sr-sec-GeV)
3.57–4.17	25.8 ± 5.3	4.90	0.76	0.256	0.12 ± 0.06
4.17–5.00	47.5 ± 7.4	5.79	1.06	0.59	0.10 ± 0.03
5.00–6.25	39.4 ± 7.7	7.09.	1.59	0.99	$(4.1 \pm 1.1)\,10^{-2}$
6.26–8.33	39.9 ± 7.7	9.14	2.65	1.21	$(2.3 \pm 0.6)\,10^{-2}$
8.33–12.5	14.3 ± 8.1	12.9	5.30	1.18	$(3.3 \pm 2.9)\,10^{-3}$
12.5–25.0	28.7 ± 9.6	22.0	15.9	1.30	$(3.0 \pm 1.1)\,10^{-3}$
25.0–50.0	0.5 ± 11.5	44.1	31.8	1.41	$(0.0 \pm 1.4)\,10^{-3}$

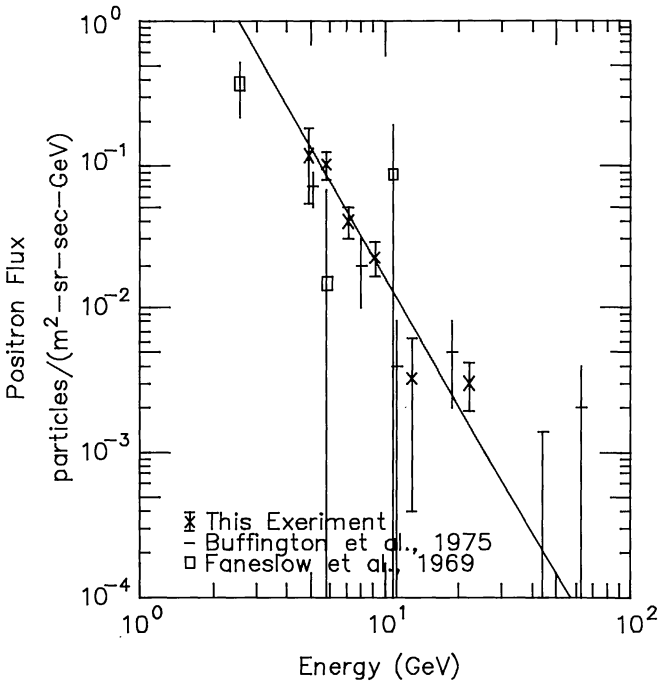

Fig. 7. Positron fluxes. Positron flux measurements from this experiment and others are shown along with the best-fit power-law representation of the differential flux. The spectral index for the fit is (-3.0 ± 0.3)

same balloon flight (Golden et al., 1984a). Buffington et al. (1975) reported a flatter spectral index of -2.3 ± 0.5 in the same energy interval for e^+. The flatter spectrum is the reason our integral fluxes are consistent with those of Buffington while their differential flux values seem smaller than ours at lower energies.

Table 7. Computation of $e^+/(e^+ + e^-)$

The $e^+/(e^+ + e^-)$ ratio was calculated using the e^+ values from Table 5 and the e^- from Table 4. Since the e^- and e^+ atmospheric background fluxes are nearly identical, the e^- fluxes in Table 4 were reduced by the atmospheric background given in Table 5. The ratio was further reduced by a factor φ which corrects for the small excess of e^+ produced by the electromagnetic cascading of the incident e^+ and e^-. The data shown are corrected to the top of the atmosphere. The highest energy interval is not included due to the very large uncertanty.

Energy (GeV)	φ	$\frac{e^+}{(e^+ + e^-)}$
4.90	1.08	0.077 ± 0.039
5.79	1.05	0.108 ± 0.024
7.09	1.05	0.068 ± 0.017
9.14	1.04	0.080 ± 0.018
12.9	1.04	0.029 ± 0.025
22.0	1.04	0.146 ± 0.049

5. Discussion

The spectral index of the positrons is steeper than the nucleons, but is nearly the same as that of the electrons (Golden et al., 1984a). This is not consistent with the expectation of the energy dependent matter traversal by cosmic rays, as deduced from the observations on heavier nuclei. However, the large flux of antiprotons ($\bar{p}$) observed at these energies (Golden et al., 1979; 1984b) has shown that the observed protons and helium nuclei could have a different origin (e.g. Stephens and Mauger, 1985). These

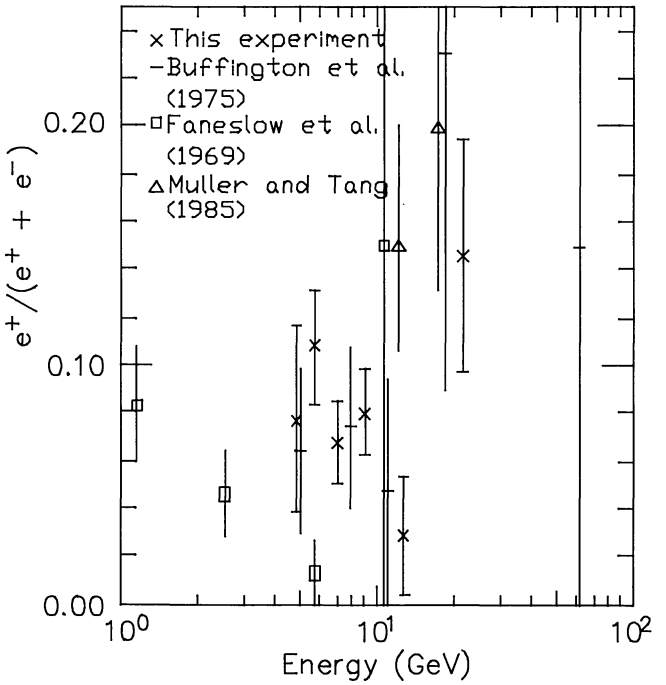

Fig. 8. The ratio $e^+/(e^+ + e^-)$. Data are shown from this experiment and previous observations. Data points with error bars that are off-plot in both vertical limits have been omitted. It is worth noting that our 21 GeV ratio is high because of the combined fluctuations of the e^+ flux above the value one might expect from a power-law fit, and the e^- flux below the expected power-law value

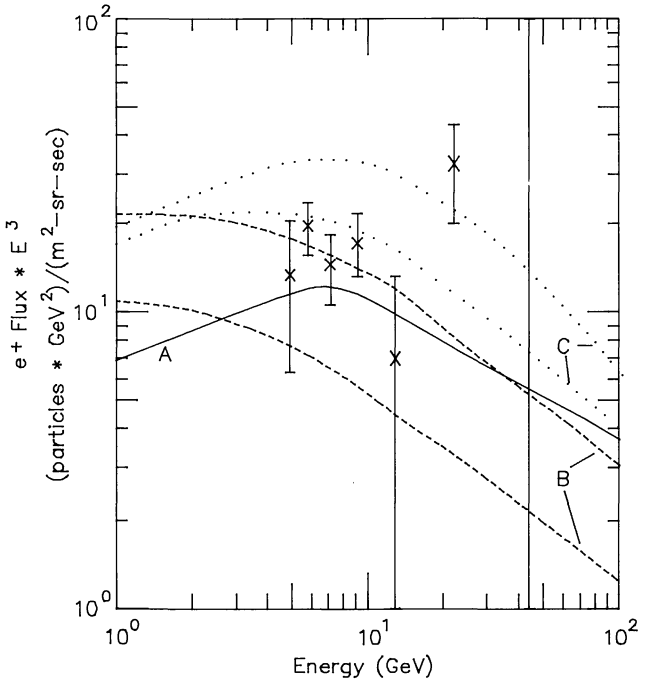

Fig. 9. Positron flux data and several theoretical predictions. The data from this experiment is shown along with: curve A – energy-dependent leak-box model (Stephens, 1981b); curves B – modified closed-galaxy model (Stephens, 1981b); curves C – shrouded supernovae (Stephens, 1981b). The predictions of the dynamical-halo model (Prothero, 1981) fall well below the data and have not been plotted

nuclei while interacting to produce $\bar{p}$ would also produce e^+. Therefore, models which explain the observed $\bar{p}$ need to be examined in the light of the observations made on e^+.

Our data are shown in Fig. 9 along with the predictions from various models. Curve A in this figure is the expected e^+ spectrum on the basis of energy-dependent leaky-box model (Stephens, 1981b). One notices that the predicted spectral shape is consistent with observations, but the absolute spectrum is smaller than the observed flux values. It is difficult at this stage to completely rule out this model due to the large errors associated with the observed flux values. However, the predictions of the dynamical halo model (Prothero, 1981) and the nested leaky-box model (Stephens, 1981b) fall well below the curves shown in the figure and hence can be ruled out. Curves labeled as B in this figure are the expected e^+ spectra on the basis of the modified closed galaxy model (Stephens, 1981b). The upper curve corresponds to $n_H = 0.2$ atom $\cdot$ cm^{-3} inside the confinement volume and the lower curve with $n_H = 0.05$ atom $\cdot$ cm^{-3}. One notices that the upper curve is consistent with the data even though the expected shape appears to be steeper than that observed. Extending the observed spectrum below and above the present energy band would be very useful to test this model. Curves labelled as C are the prediction of supernova explosions in clouds (Stephens, 1985). The upper curve corresponds to a magnetic field strength in the cloud, which is compressed from a 4 μG ambient field, and the lower curve is for an ambient field of 8 μG. It is possible to obtain a better agreement with the data on the basis of this model if one invokes higher radiative losses for electrons inside the supernova envelopes.

It appears from the above discussion that the observed e^+ spectrum is consistent with the $\bar{p}$ observations and that these particles could have a common origin by secondary production from collisions of cosmic ray nuclei. It is very essential to improve the quality of the data and extend the spectrum to lower and higher energies in order to distinguish between various models.

Acknowledgements. During the initial phases, this work was performed at the National Aeronautics and Space Administration's Johnson Space Center. The Lockheed Electronics Corporation acted as the principal support contractor during this period. We are very grateful to those Lockheed and NASA employees which helped get the program started. Since the relocation of the group to New Mexico State University (NMSU). NASA has supported the work through contract NAS9-15660 and grant NAGW-110. Personnel from the NMSU Electrical and Computer Engineering Department, Engineering Research Center and Physical Science Laboratory have given enthusiastic and essential support. Thanks to all of you that have helped, especially to Mr. R.F. Park. Thanks are certainly due to the staff of the National Scientific Balloon Facility, which provided the balloon flight support services. One of us (SAS) wishes to thank NMSU for the hospitality during the final phase of the analysis.

References

Badhwar, G.D., Golden, R.L.: 1974, *Nature* **126**

Badhwar, G.D., Golden, R.L., Brown, M.L., Lacy, J.L.: 1975, *Astrophys. Space Sci.* **37**, 283

Buffington, A., Orth, C.D., Smoot, G.P.: 1975, *Astrophys. J.* **199**, 699
Faneslow, J.L., Hartman, R.C., Hildebrand, R.H., Meyer, P.: 1969, *Astrophys. J.* **158**, 771
Golden, R.L., Badhwar, G.D., Lacy, J.L., Zipse, J.E.: 1978, *Nuclear Instr. and Meth.* **148**, 179
Golden, R.L., Horan, S., Mauger, B.G., Badhwar, G.D., Lacy, J.L., Stephens, S.A., Daniel, R.R., Zipse, J.E.: 1979, *Phys. Rev. Letters* **43**, 1196
Golden, R.L., Mauger, B.G., Badhwar, G.D., Lacy, J.L., Stephens, S.A., Daniel, R.R.: 1984a, *Astrophys. J.* **287**, 622
Golden, R.L., Mauger, B.G., Nunn, S., Horan, S.: 1984b, *Astrophys. Letters* **24**, 75
Golden, R.L., Mauger, B.G., Horan, S., Badhwar, G.D., Lacy, J.L., Zipse, J.E., Daniel, R.R., Stephens, S.A.: 1985, *Proc. 19th International Cosmic Ray Conference*, La Jolla, **2**, 374
Lacy, J.L., Lindsey, R.S.: 1974, *Nuclear Instr. and Meth.* **119**, 483
Mauger, B.G.: 1981, Ph.D. thesis, New Mexico State University.
Muller, D., Tang, J.: 1985, *Proc. 19th International Cosmic Ray Conference*, La Jolla, **2**, 378
Protheroe, R.J.: 1981, *Astrophys. J.* **251**, 387
Stephens, S.A.: 1981a, *Proc. 17th International Cosmic Ray Conference*, Paris, **4**, 282
Stephens, S.A.: 1981b, *Proc. 17th International Cosmic Ray Conference*, Paris, **2**, 214
Stephens, S.A.: 1985, *Proc. 19th International Cosmic Ray Conference*, La Jolla, **2**, 390
Stephens, S.A., Mauger, B.G.: 1985, *Astrophys. Space Sci.* **110**, 337